Thin Solid Films 519 (2011) 5194–5198

Contents lists available at ScienceDirect

Thin Solid Films

journal homepage: www.elsevier.com/locate/tsf

Nanostructured thin films for anti-reflection applications

J.Y. Chen, K.W. Sun *

Department of Applied Chemistry, National Chiao Tung University, Hsinchu, Taiwan

ARTICLE INFO

Available online 19 January 2011

Keywords:
Nanoimprint
Anti-reflection
Sub-wavelength structure

ABSTRACT

Anti-reflection (AR) thin films composed of ordered arrays of tapered nanostructures on the surface of PMMA and silicon, through the hot-embossing nanoimprint of polymer using molds prepared from e-beam lithography and hydrothermally grown ZnO nanorod arrays. The use of PMMA and ZnO nanorod thin films allows the formation of anti-reflection structures on a curved or flat surface to effectively suppress the reflectance of the incident light. It provides a simple and low-cost means for large-scale use in the production of AR layers for improving optical and optoelectronic device performance, such as solar cells and photodetectors. A drastic reduction in the reflectivity of the AR layer over a broad spectral range was demonstrated. In addition, the great improvement on the light harvest efficiency of the solar cells by over 30% using the nanostructured AR layer was validated.

1. Introduction

An anti-reflection (AR) layer is a type of coating applied to the surface of a material to reduce light reflection and to increase light transmission. The AR layers have attracted increasing interest owing to their applicability to various types of optical and optoelectronic devices, such as solar cell, planar displays, glasses, prisms, videos, and camera monitors. Surface-relief gratings with a size smaller than the wavelength of light, named sub-wavelength structure (SWS), behave as antireflection surfaces. By using a mechanically continuous wavelike grating (e.g., pyramidal, triangular, and conical shapes), the SWS grating acts as a surface possessing a gradually and continuously changing refractive index profile from the air to the substrate. In these AR structures, the ordered array of tapered pillar structures can effectively suppress the reflection on the surface [1–5]. Tapered SWSs have been fabricated through different methods [6–8]. Ishimori et al. used an e-beam lithography technique to generate triangular structures in the photoresist and utilized a focused SF_6 fast atom beam (FAB) to produce tapered sub-wavelength structures. However, the fabrication costs, which involve either electron-beam lithography or various etching processes, can be significant. Recently, versatile SWSs have emerged as promising candidates for AR coatings such as etching with self-aggregated nanodot mask [9,10], moth-eye like fabrication [11,12], nanorod fabrication [13–15], and nanostructures employing oblique-angle deposition methods [16,17].

Nanoimprint lithography (NIL), which was first demonstrated by Chou et al. [18], is a lithography technique performed by pressing the patterned mold so that it makes contact with the polymer resist directly. This technology provides a different way to fabricate nanostructures with easy processes, high throughput, and low cost. It is capable of replicating patterns with a linewidth below 10 nm in a parallel manner [19]. NIL has been used to produce large-area polymer sheets with SWS as AR layers [20,21].

More recently, ZnO becomes attractive as an alternative of a dielectric AR layer material because of its good transparency, appropriate refractive index, and ability to form textured coating via anisotropic growth [22–29]. Various physical, chemical, and electrochemical deposition techniques have been explored to create oriented arrays of ZnO nanorod. For instance, pulsed laser deposition [22], metal-organic chemical vapor deposition [23], and epitaxial electrodeposition [24] have been achieved in the fabrication of ZnO nanorod arrays. However, the fabrication costs can be significant. Recently, the solution synthesis of ZnO nanorod arrays has been demonstrated as a simple, low temperature, and low-cost method [25–28]. Vertically aligned ZnO nanorod arrays have been used to produce AR layers [29,30].

In this paper, we report the AR properties of both the nanostructured PMMA AR thin films fabricated by NIL technology and the highly textured ZnO nanorod layers fabricated with the solution growth technique. Fabrication and tests of the AR properties on the real Si P–N junction solar cell devices incorporated were also demonstrated. The process described in the present report can be applied on various optical and optoelectronic devices and provide a promising technique for the fabrication of high-efficiency devices.

2. Material and experimental methods

2.1. Spin-coating replication/hot-embossing NIL processes

The flow charts of the mold fabrication and spin-coating replication/hot-embossing NIL processes are shown in Fig. 1. A silicon

* Corresponding author.
E-mail address: kwsun@mail.nctu.edu.tw (K.W. Sun).

0040-6090/$ – see front matter © 2011 Elsevier B.V. All rights reserved.
doi:10.1016/j.tsf.2011.01.110

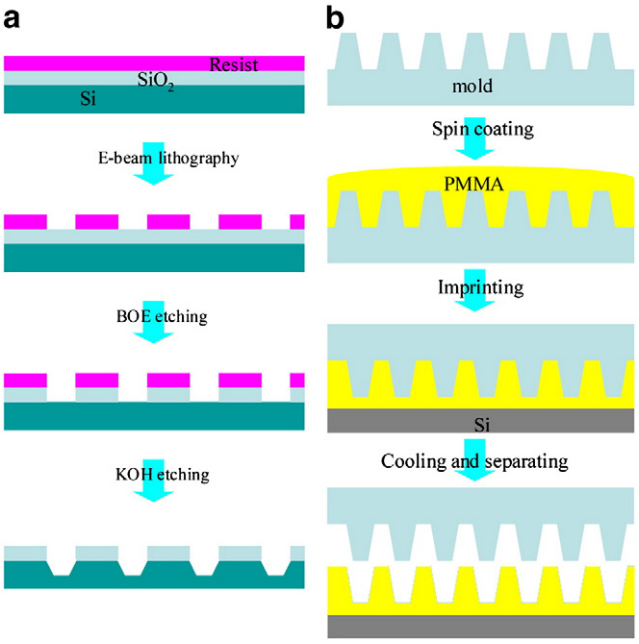

Fig. 1. Steps used for (a) mold fabrication and (b) spin-coating replication/hot-embossing processes.

wafer was used as the substrate for the hot-embossing NIL mold fabrication. The substrate surface was first cleaned up with ACE, IPA, and D.I. water by ultrasonic agitation. A 50 nm SiO_2 was deposited on the surface as the mask of the wet etching. The sample was then coated with ZEP-520A photoresist and exposed to the electron beam. 2D patterns within a square area measuring 5 mm by 5 mm, as shown in Fig. 2(a), were defined on the mold surface with a linewidth of 80 nm and pitches of 1500 nm. After developing with ZED-N50, the e-beam defined patterns were first chemically etched in a solution mixture of HF and NH_4F (1:6) for 15 s to transfer the pattern on the SiO_2 mask. Then, the entire mold was dipped into a KOH solution mixture with 30% KOH and 20% IPA for 1–5 min at 80 °C. Due to the transverse etching of the acid solution and the anisotropic etching of the KOH solution, the wet etching process resulted in tapered nano-post arrays as shown in Fig. 2(b). For the mold with pitches of 1500 nm, the structures formed octagonal-shaped cones with a flat top. The depths of the mold were all 700–900 nm. The reflection spectrum of the mold, as shown in Fig. 2(c), was measured for wavelengths that ranged from 300 to 1000 nm. The spectrum of the mold showed significantly reduced reflectance (<6%) through the entire wavelength range at normal incidence.

The spin-coating replication/hot-embossing techniques and a home-made pneumatic nanoimprintor were used to transfer the patterns on the molds to a PMMA layer on a Si template. Before the imprinting processes, the mold was first placed in a closed bottle filled with vaporized 1H,1H,2H,2H-perfluoro-octyltrichlorosilane at 250 °C for 1 h. The mold release agent coated on the mold can facilitate the separation of the replica from the mold after the imprinting process. A layer of PMMA of 950 K molecular weight and solid contents of 15% in anisole was spin-coated on the mold at 1000 rpm. The substrate and mold were then combined and placed on the sample stage in our home-made nanoimprintor. The PMMA films were hot-embossed at a temperature of 120 °C under a pressure of 0.4 kg/cm^2. The pressure was relieved and the sample was de-molded after the stage has cooled down to room temperature.

2.2. Preparation of ZnO nanorod arrays on a Si template

The ZnO nanorods used in the present experiment were grown on Si substrate and poly-Si solar cell by the aqueous chemical growth

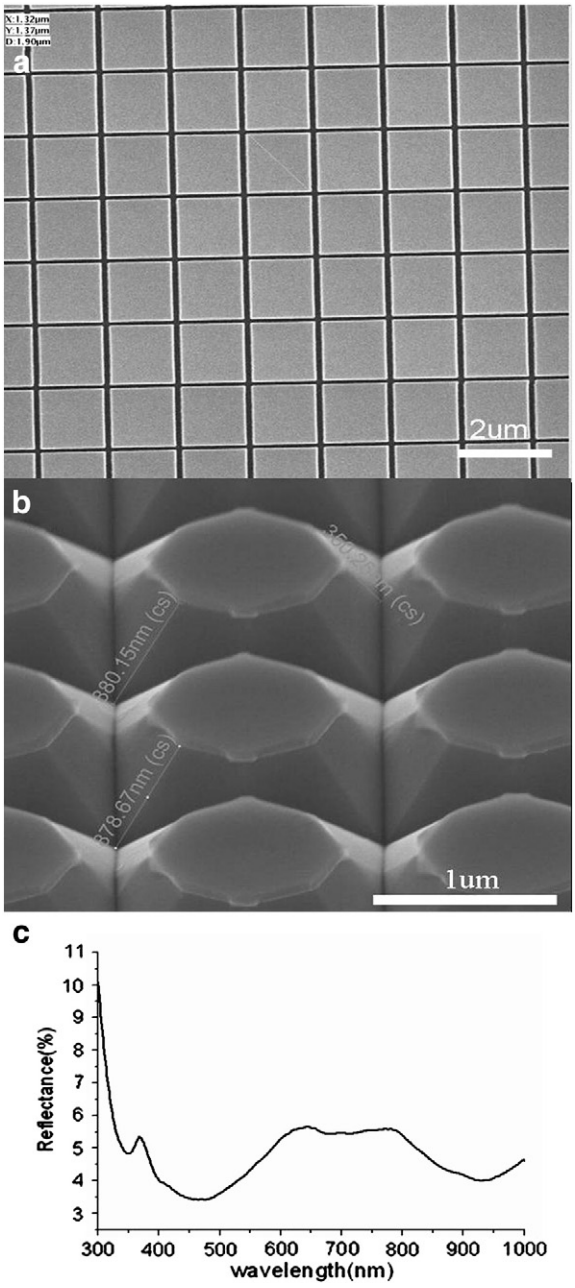

Fig. 2. SEM images of (a) E-beam defined grating patterns with pitches of 1500 nm. (b) Fabricated silicon molds after chemical wet etching. (c) Reflection spectra of the mold and bare Si.

method [25,28]. Before the growth process, the substrates were coated with a ZnO nanoparticle layer by the sol–gel preparation as the seeding layer. The substrate surface was first cleaned up with ACE, IPA, and D.I. water by ultrasonic agitation. The decomposition or hydrolysis of zinc salts is a well-established method to fabricate a ZnO nanoparticle. First, the zinc acetate dihydrate and monoethanolamine were dissolved in the 2-methoxyethanol solution, which served as the coating solution, at room temperature. The clean substrates were spin-coated with the solution at 1000–5000 rpm to ensure a uniform coverage of seeds and then the substrates were heated at 300 °C in air atmosphere for 1 h to yield layers of ZnO seeds. The solution for growing the ZnO nanorods was prepared by mixing the zinc nitrate hexahydrate with hexamethylenetetramine using the same molar concentration. The molar concentration was varied from 0.01 M to 0.04 M. After the two solutions were mixed, the substrates were

immersed inside the solution at 90 °C for 120 min to 300 min. After the growth process was completed, the substrates were cleaned in D.I. water to remove the residual salt and amino complex and finally dried in air.

The surface morphology of the samples and size distribution of the vertically aligned ZnO nanorod arrays were characterized by scanning electron microscope (SEM) and X-ray diffraction (XRD). The reflection spectra of the samples were measured for wavelengths ranging from 190 to 1000 nm.

3. Results and discussion

3.1. AR performance of nanostructured PMMA layers

The resulting pattern on the PMMA layers after the imprinting processes is shown in Fig. 3(a). The nanostructures after the NIL have the same depth as the molds. The ability of the PMMA to fill completely the molds when it was spin-coated on the mold accounts for this. In Fig. 3(b), the reflection spectra and the comparisons of the AR performance of the nanostructured PMMA layers with bare Si are shown. In general, the tapered cone structure with a very steep angle and a polygon base can lead to the gradual and continuous change of the refractive index profile from the air to the substrate [6–8]. Therefore, it can greatly reduce the reflection from the surface.

In order to test the AR performance of the nanostructured layer, the PMMA thin film was peeled off from the Si template and directly transferred onto the commercially available poly-Si solar cell surface. It should be noted that, due to the metal contact on the cell, the PMMA thin film could not completely sit flat on the surface. The reflectivity of the PMMA film on the solar cells was increased slightly than when sitting on a flat surface [see Fig. 3(c)]. The poly-Si solar cell with a PMMA thin film was characterized under the air mass 1.5 global (AM 1.5G) illumination condition and was compared to the cell that did not undergo the antireflection treatment. The measured current–voltage characteristics are shown in Fig. 3(d). The short-circuit current was enhanced by 23% due to the PMMA nanostructured film. The light conversion efficiency of the solar cells was improved from 10.4% to 13.5% with the use of the PMMA thin film as the AR layer.

3.2. AR properties of ZnO nanorod arrays

The geometries of the as-grown ZnO nanorods can be tuned to varying degrees by changing the growth time, seed density, and solution composition. AR performance was optimized by taking the following procedure to control ZnO nanorod morphology on Si substrates.

Fig. 4(a) shows the SEM image of the vertically aligned ZnO nanorod arrays on Si substrates with a growth time of 180 min when the growth solution with a molar concentration 0.04 M was used and the zinc acetate solution spin coating rotation rate was fixed at 5000 rpm. The arrays consisted of nanorods with diameters of 70–80 nm and lengths of ~150 nm. The density of ZnO nanorod arrays was around 1.2×10^{10} cm^{-2}. In Fig. 4(b), the reflection spectrum and the comparisons of the AR performance of the above vertically aligned ZnO nanorod arrays with bare Si are shown. The figure shows that the reflectance of the ZnO nanorods was reduced to about 3%–4% at a wavelength of 667 nm. The X-ray diffraction (XRD) patterns of the ZnO nanorods with different growth times are illustrated in Fig. 4(c). Three pronounced wurtzite ZnO diffraction peaks, (1 0 0), (0 0 2), and (1 0 1) appear at $2\theta = 31.89°$, 34.65°, and 36.3° [27]. The XRD spectra of all ZnO nanorods revealed a strong (0 0 2) peak, indicating that the nanorods have high orientation with the c-axis vertical to the substrate surface.

By varying experimental parameters, we have learned that the variations in growth conditions strongly influenced the morphology of the textured ZnO nanorods and had a great effect on the AR layer

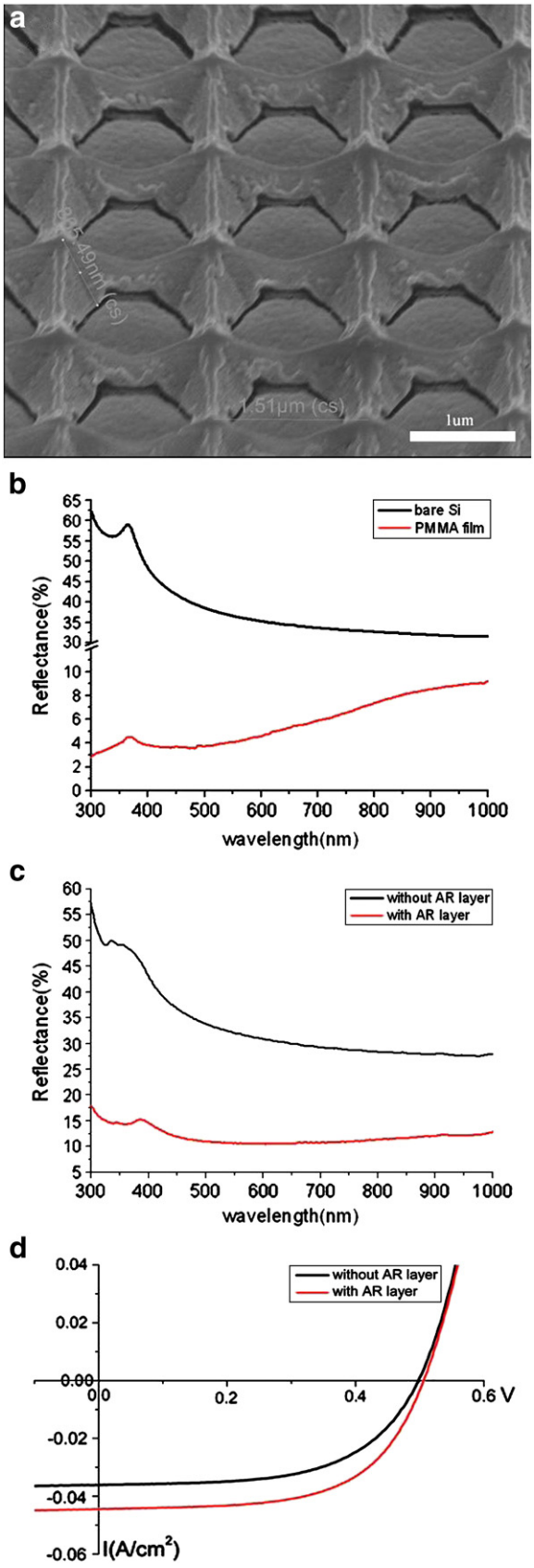

Fig. 3. (a) SEM images of the replicated PMMA sub-wavelength structures with pitches of 1500 nm. (b) Reflection spectra of the replicated PMMA sub-wavelength structures and bare Si. (c) Reflection spectra of the poly-Si P–N junction solar cells with and without the nanostructured PMMA layer. (d) Current–voltage characteristics of the solar cells with and without the nanostructured PMMA layer.

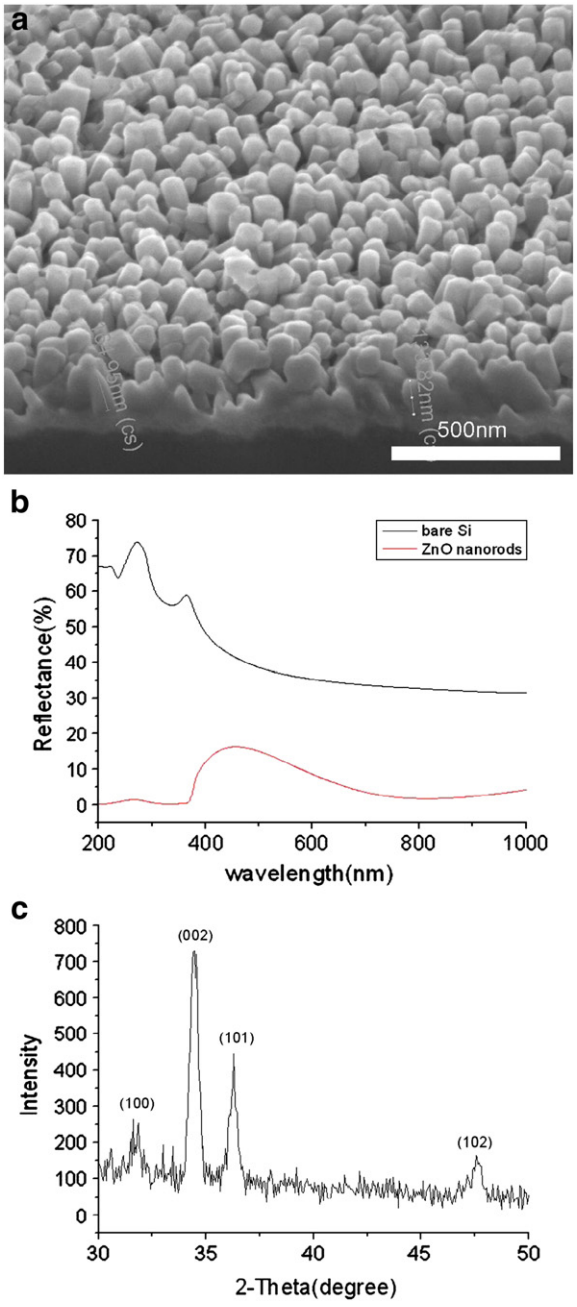

Fig. 4. (a) SEM images of the vertically aligned ZnO nanorod arrays on Si substrates with a growth time of 180 min, a molar concentration 0.04 M, and a spin coating rotation rate of 5000 rpm. (b) Reflection spectra of the layer with ZnO nanorod arrays and bare Si. (c) X-ray diffraction patterns of ZnO nanorod arrays.

performance due to the differences in lengths, densities, and diameters of the nanorods. Therefore, the optimized growth parameters of 180 min growth time, 5000 rpm spin coating rotation rate, and a solution concentration of 0.04M were finally reached and were used to demonstrate the growth of the ZnO nanorod arrays on the poly-Si solar cell as the AR layer. Comparisons of the resulting reflection spectra from the ZnO nanorod AR layer with the bare poly-Si solar cell are shown in Fig. 5(a). The figure shows that the reflectivity is greatly reduced with the ZnO nanorod arrays. The poly-Si solar cell with ZnO nanorods was characterized under the AM 1.5G illumination condition and was compared to the cell that did not undergo the AR treatment. The measured current–voltage characteristics are shown in Fig. 5(b). Although the ZnO AR layer deposited on the solar cell surface absorbs the UV light (above 380 nm). However,

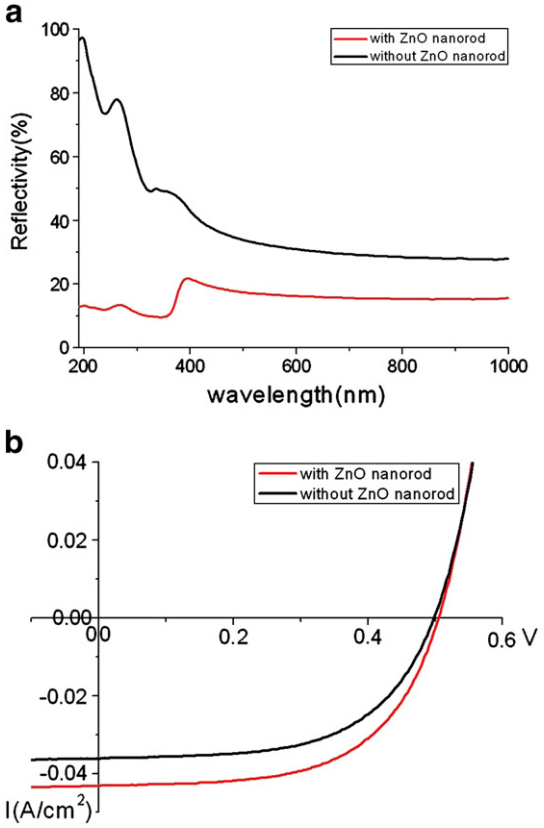

Fig. 5. (a) Reflectance of the solar cell devices with and without the AR layer of ZnO nanorod arrays. (b) I–V characteristics of the solar cells with and without the AR layers.

due to lack of the electrical field, the photogenerated carriers have little chance to get separated and are quickly recombined. Therefore, they cannot be collected by the electrodes and contribute to the total photocurrent. The short-circuit current was enhanced by 20% due to the presence of the ZnO nanorod layer. The light conversion efficiency of the solar cells was improved from 10.4% to 12.8% with the use of aligned ZnO nanorod arrays as the AR layer.

4. Conclusions

In summary, we present simple and low-cost methods to produce AR polymer thin films with 2D periodically nanostructures using the spin-coating replication/hot-embossing nanoimprint lithography, and vertically aligned ZnO nanorod arrays by the aqueous chemical growth method. The structures can reduce surface Fresnel reflection over a broad spectral range. This technology was used for AR applications in solar cells for improving their light conversion efficiency. The light harvest efficiency of the poly-Si solar cells was improved by over 30% with the AR layers. It can also find broad applications in other types of electro-optical devices.

Acknowledgements

This work was supported by the National Science Council of Republic of China under contract nos. NSC 96-2112-M-009-024-MY3, and NSC 96-2120-M-009-004, and the MOE ATU program.

References

[1] S.J. Wilson, M.C. Hutley, Opt. Acta 29 (1982) 993.
[2] M.E. Motamedi, W.H. Southwell, W.J. Gunning, Appl. Opt. 31 (1992) 4371.
[3] P. Lalanne, G.M. Morris, Nanotechnology 8 (1997) 53.
[4] T. Glaser, A. Ihring, W. Morgenroth, N. Seifert, S. Schroter, V. Baier, Microsyst. Technol. (2005) 86.

[5] W.L. Min, A.P. Betancourt, P. Jiang, B. Jiang, Appl. Phys. Lett. 92 (2008) 141109.
[6] M. Ishimori, Y. Kanamori, M. Sasaki, K. Hane, Jpn. J. Appl. Phys. 41 (2002) 4346.
[7] Y. Kanamori, M. Sasaki, K. Hane, Opt. Lett. 24 (1999) 1422.
[8] K. Hadob´as, S. Kirsch, A. Carl, M. Acet, E.F. Wassermann, Nanotechnology 11 (2000) 161.
[9] S. Wang, X.Z. Yu, H.T. Fan, Appl. Phys. Lett. 91 (2007) 061105, 3 pages.
[10] G.-R. Lin, Y.-C. Chang, E.-S. Liu, H.-C. Kuo, H.-S. Lin, Appl. Phys. Lett. 90 (2007) 181923, 3 pages.
[11] C.-H. Sun, W.-L. Min, N.C. Linn, P. Jiang, B. Jiang, Appl. Phys. Lett. 91 (2007) 231105, 3 pages.
[12] C.-H. Sun, P. Jiang, B. Jiang, Appl. Phys. Lett. 92 (2008) 061112, 3 pages.
[13] J. Zhu, Z. Yu, G.F. Burkhard, C.-M. Hsu, S.T. Connor, Y. Xu, Q. Wang, M. McGehee, S. Fan, Y. Cui, Nano Lett. 9 (2009) 279.
[14] E. Garnett, P. Yang, Nano Lett. 10 (2010) 1082.
[15] Y. Lu, A. Lal, Nano Lett. 10 (2010) 4651.
[16] M.-L. Kuo, D.J. Poxson, Y.S. Kim, F.W. Mont, J.K. Kim, E.F. Schubert, S.-Y. Lin, Opt. Lett. 33 (2008) 2527.
[17] P. Yu, C.-H. Chang, C.-H. Chiu, C.-S. Yang, J.-C. Yu, H.-C. Kuo, S.-H. Hsu, Y.-C. Chang, Adv. Mater. 21 (2009) 1618.
[18] S.Y. Chou, P.R. Krauss, J. Renstrom, Appl. Phys. Lett. 67 (1995) 3114, 3 pages.
[19] V. Boerner, S. Abbott, B. Blasi, A. Gombert, W. Hobfeld, SID. Symp. Digest 34 (2003) 68.
[20] C.-J. Ting, M.-C. Huang, H.-Y. Tsai, C.-P. Chou, C.-C. Fu, Nanotechnology 19 (2008) 205301, 5 page.
[21] Y. Kanamori, E. Roy, Y. Chen, Microelectron. Eng. 78–79 (2005) 287.
[22] Mitsuhisa Kawakami, A.B. Hartanto, Y. Nakata, T. Okada, Jpn. J. Appl. Phys. 42 (2003) L 33.
[23] K.-S. Kim, H.W. Kim, Phys. B 328 (2003) 368.
[24] R. Liu, A.A. Vertegel, E.W. Bohannan, T.A. Sorenson, J.A. Switzer, Chem. Mater. 13 (2001) 508.
[25] L.E. Greene, M. Law, D.H. Tan, M. Montano, J. Goldberger, G. Somorjai, P. Yang, Nano Lett. 5 (2005) 1231.
[26] Y. Tak, K. Yong, J. Phys. Chem. B 109 (2005) 19263.
[27] Z. Chen, L. Gao, J. Cryst. Growth 293 (2006) 522.
[28] M. Riaz, A. Fulati, G. Amin, N.H. Alvi, O. Nur, M. Willander, J. Appl. Phys. 106 (2009) 034309.
[29] Y.J. Lee, D.S. Ruby, D.W. Peters, B.B. McKenzie, J.W.P. Hsu, Nano Lett. 8 (2008) 1501.
[30] T.H. Ghong, Y.D. Kim, E. Ahn, E. Yoon, S.J. An, G.–.C. Yi, Appl. Surf. Sci. 255 (2008) 746.